

Nanoscale

Accepted Manuscript



This is an *Accepted Manuscript*, which has been through the Royal Society of Chemistry peer review process and has been accepted for publication.

Accepted Manuscripts are published online shortly after acceptance, before technical editing, formatting and proof reading. Using this free service, authors can make their results available to the community, in citable form, before we publish the edited article. We will replace this *Accepted Manuscript* with the edited and formatted *Advance Article* as soon as it is available.

You can find more information about *Accepted Manuscripts* in the [Information for Authors](#).

Please note that technical editing may introduce minor changes to the text and/or graphics, which may alter content. The journal's standard [Terms & Conditions](#) and the [Ethical guidelines](#) still apply. In no event shall the Royal Society of Chemistry be held responsible for any errors or omissions in this *Accepted Manuscript* or any consequences arising from the use of any information it contains.



Stereo-epitaxial Growth of Single-crystal Ni Nanowires and Nanoplates from Aligned Seed Crystals

Hyoban Lee,^a Youngdong Yoo,^{a,b} Taejoon Kang,^c Jiyoung Lee,^a Eungwang Kim,^a Xiaosheng Fang,^d Sungyul Lee,^{*e} and Bongsoo Kim,^{*a,f}

Received 00th January 20xx,
Accepted 00th January 20xx

DOI: 10.1039/x0xx00000x

www.rsc.org/

Epitaxially grown anisotropic Ni nanostructures are promising building blocks for the development of miniaturized and stereo integrated data storage kits because they can store multiple magnetic domain walls (DWs). Here, we report stereo-epitaxially grown single-crystalline Ni nanowires (NWs) and nanoplates, and their magnetic properties. Vertical and inclined Ni NWs were grown on the center and edge regions of *c*-cut sapphire substrates, respectively. Vertical Ni nanoplates were grown on *r*-cut sapphire substrates. The morphology and growth direction of Ni nanostructures can be steered by seed crystals. Cubic Ni seeds grow into vertical Ni NWs, tetrahedral Ni seeds grow into inclined Ni NWs, and triangular Ni seed grow into vertical Ni nanoplates. The shapes of the Ni seeds are determined by the interfacial energy between the bottom plane of the seeds and the substrates. As-synthesized Ni NWs and nanoplates have blocking temperature values greater than 300 K at 500 Oe, verifying that these Ni nanostructures can form large magnetic DWs with high magnetic anisotropy properties. We anticipate that epitaxially grown Ni NWs and nanoplates will be used in various types of 3-dimensional magnetic devices.

1. Introduction

Ferromagnetic nanowires (NWs) have been regarded as attractive building blocks for applications in magnetic storage devices, nanoelectronics, and spintronics^{1,2} because a single ferromagnetic NW with a high surface-to-volume ratio can store multiple magnetic domain walls (DWs). In particular, aligned ferromagnetic NWs can offer significant advantages for the fabrication of 3-dimensional magnetic devices such as racetrack memory.³ Nickel (Ni), one of the representative ferromagnetic materials, has been widely used in memory chips,⁴⁻⁶ magnetics,^{7,8} fuel cells,^{9,10} catalysts,¹¹⁻¹³ and batteries.¹⁴ Because the aligned Ni NW arrays enable both miniaturization and stereo-integration of data storage kits, it is extremely important to synthesize well-aligned Ni NW arrays.

Wet-chemical approaches using anodic aluminum oxide (AAO) templates enable Ni NWs to grow up vertically on substrate.¹⁵⁻¹⁷ Since these NWs are often tangled with each other

and form bundles after the removal of the AAO templates, individual control of the Ni NWs in a spin device is hardly possible. In addition, Ni NWs electrochemically formed have rough surfaces, limiting efficient transport of magnetic spins and the formation of well-defined magnetic DWs. Lithographic approaches have also been employed for the fabrication of Ni NWs. However, such approaches are complex, time consuming, and expensive.¹⁸ Recently, Chan *et al.* successfully employed chemical vapor deposition (CVD) techniques to synthesize vertical single-crystal Ni NWs on amorphous SiO₂ substrate.^{19,20} This study stimulated us to develop a morphology and growth direction controllable synthetic method of Ni nanostructures in vapor phase.

Here, we report epitaxially grown Ni NWs and nanoplates in vapor phase, and their magnetic properties. Vertical and inclined Ni NWs were synthesized on *c*-cut sapphire substrates and vertical Ni nanoplates were synthesized on *r*-cut sapphire substrates. The morphology and growth direction of Ni nanostructures were steered by Ni seed crystals, which were formed on the substrates by the favorable interfacial energy between the bottom plane of the seeds and the substrates.²¹ In this experiments, cubic Ni seeds grew into vertical Ni NWs, tetrahedral Ni seeds grew into inclined Ni NWs, and triangular Ni seed grew into vertical Ni nanoplates. Ni NWs and nanoplates are single-crystalline and well-faceted with atomically smooth surfaces. The magnetic property measurements from the vertical Ni NW and nanoplate arrays show that the blocking temperatures (T_B) is above room temperature at 500 Oe, demonstrating their suitability for potential use in future 3-dimensional magnetic memory.

^a Department of Chemistry, KAIST, Daejeon 34141, Korea. E-mail: bongsoo@kaist.ac.kr

^b Department of Chemistry, University of Minnesota, Minneapolis, Minnesota 55455, USA

^c BioNanotechnology Research Center and BioNano Health Guard Research Center, KRIBB, Daejeon 34141, Korea

^d Department of Materials Science Fudan University, Shanghai 200433, P. R. China

^e Department of Applied Chemistry, Kyunghee University, Kyungki-do 17104, Korea. E-mail: sylee@khu.ac.kr

^f KAIST Institute for the NanoCentury, KAIST, Daejeon 34141, Korea

† Electronic Supplementary Information (ESI) available. See DOI: 10.1039/x0xx00000x

2. Experimental section

2.1 Synthesis of Ni NWs and Nanoplates

Ni NWs and Ni nanoplates are synthesized in a horizontal hot wall two-zone furnace employing a 1 in. diameter inner quartz tube (Fig. S1†). NiCl₂ precursor (anhydrous, 0.02 ~ 0.04 g, 99.99 %, Sigma-Aldrich) in alumina boat is placed at the middle position of upstream zone, and 5 × 5 mm² sized *c*- or *r*-Al₂O₃ substrates (MTI Corporation, USA) are placed at the 15 ~ 20 cm away from the precursor. The NiCl₂ is heated at 770 ~ 840 °C for 25 min under 80 ~ 100 sccm of Ar flow rate. In order to decompose NiCl₂ efficiently and prevent the oxidation of Ni nanostructures, preheating step was accomplished at 200 ~ 300 °C.

2.2 Characterization

Field-emission SEM images were taken on a Philips XL30S with Pt coating to avoid charging effect during SEM observation. TEM images including SAED patterns were taken on a TECNAI F30 TEM operated at 200 kV. For TEM analysis, we sonicated the as-grown substrate in ethanol solution for 5 min to detach the Ni nanostructures. After Ni nanostructures were dispersed in ethanol, we dropped the solution on a holey carbon coated copper grid. After Ni nanostructures were dispersed in ethanol, we dropped this solution on a holey carbon coated copper grid.

3. Results and discussion

3.1 Ni NWs Synthesis of epitaxially grown Ni nanostructures in vapor phase

Ni NWs and nanoplates were epitaxially synthesized on *c*-cut sapphire (*c*-Al₂O₃) and *r*-cut sapphire (*r*-Al₂O₃) substrates, respectively, using a horizontal quartz tube furnace system (Fig. S1†). Anhydrous NiCl₂ was employed as a precursor and simply modified van Arkel method was used for the separation and purification of Ni.^{22,23} In the quartz tube, NiCl₂ is evaporated, transported to the sapphire substrates by a carrier gas, and decomposed into Ni and Cl₂. After reaction time of 25 min, single-crystalline Ni NWs and nanoplates are grown on *c*-Al₂O₃ and *r*-Al₂O₃ substrates, respectively.

3.2 Vertical and inclined Ni nanowires on *c*-Al₂O₃ substrates

Fig. 1a-d show scanning electron microscopy (SEM) images of vertical and inclined Ni NWs on *c*-Al₂O₃ substrates. The vertical Ni NWs were grown at the center of the substrate, and the inclined NWs were grown at the edges (Fig. S2†). Both NWs are rectangular parallelepiped having 100-500 nm of diameter and ~10 μm of length. The diameter can be controlled by changing a source temperature or reaction time. The vertical Ni NWs exhibited two orientations with an angle of 45°, as marked by the yellow and red circles in Fig. 1c. The insets in Fig. 1c and 1d show the different bottom end structures of the vertical and inclined Ni NWs, indicating that the vertical and inclined Ni NWs grew from different seed structures. Distinct lattice fringes and selected-area electron diffraction (SAED) patterns obtained via transmission electron microscopy (TEM) confirm that

the Ni NWs are single-crystalline and have a growth direction of <100> (Fig. 1e and 1f).

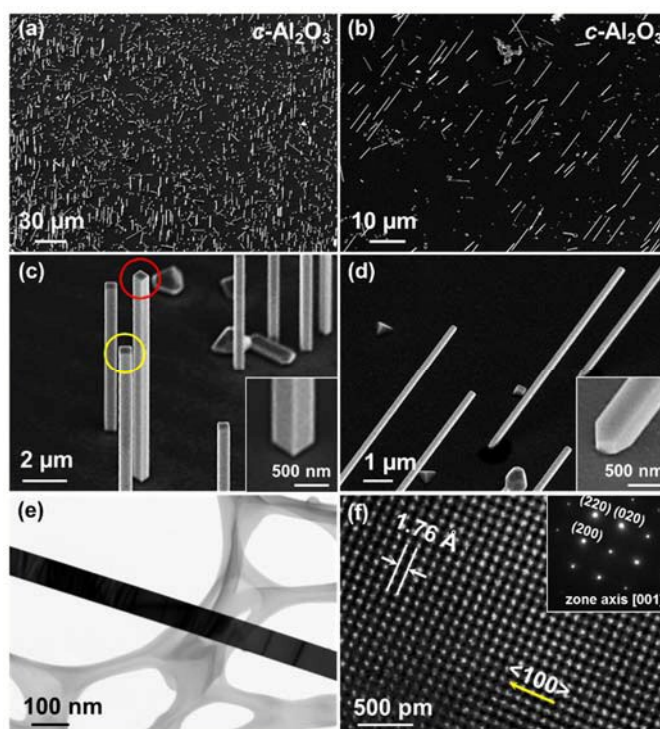


Fig. 1 45°-tilted SEM images of (a, c) vertical and (b, d) inclined Ni NWs on *c*-Al₂O₃ substrates. The Ni NWs have well-defined facets, 100-500 nm diameters, ~10 μm lengths, and rectangular parallelepiped shapes. Magnified SEM image of the vertical Ni NWs show that they have two types of orientations with an angle of 45° (yellow and red circles). The insets show the bottom end structures of the Ni NWs. The different bottom end structures of the vertical and inclined Ni NWs suggest that they are grown from different seed crystals. (e, f) HRTEM image and SAED patterns of Ni NWs clearly indicate that the Ni NWs are single-crystalline and have growth direction of <100>.

To investigate the Ni NW growth mechanism, we observed Ni seeds on the NWs grown *c*-Al₂O₃ substrates. Cubic Ni seed crystals are observed around the vertical Ni NWs (Fig. 2a). Similar to the vertical Ni NWs, cubic Ni seeds have two orientations with an angle of 45° (inset of Fig. 2a). The same alignments and tip structures of vertical Ni NWs and cubic Ni seed crystals suggest that the vertical Ni NWs grow from the cubic Ni seed crystals. Fig. 2b is a cross-sectional TEM image of a single cubic Ni seed on a *c*-Al₂O₃ substrate. The sample was fabricated using focused ion beam (FIB) milling, and the yellow dashed line in Fig. 2a is the cut direction. From the cross-sectional TEM analysis, we observed that the cubic Ni seed crystal is enclosed by {100} facets and is single-crystalline without any internal twin planes.

Fig. 2c shows a high-resolution TEM (HRTEM) image and fast Fourier transform (FFT) patterns of the cyan square region in Fig. 2b. The Ni (100) plane is formed epitaxially on the Al₂O₃ (0001) plane. The schematic of the atomic planes at the epitaxial interface between Ni (001) and Al₂O₃ (0001) planes show that the interfacial energy between these two planes is highly favorable (Fig. 2d). Seven layers of Ni and 3 layers of Al₂O₃ have 0.32% domain-matched misfit along the Ni [100]//Al₂O₃ <100> direction (the lattice spacing of the Ni (100) planes is 1.76 Å and that of the Al₂O₃ (100) planes is

4.12 Å).^{24,25} Additionally, 4 layers of Ni and 3 layers of Al₂O₃ have 1.40% domain-matched misfit along the Ni [010]//Al₂O₃ <11 $\bar{2}$ 0> direction (the lattice spacing of the Ni (010) planes is 1.76 Å and that of the Al₂O₃ (11 $\bar{2}$ 0) planes is 2.38 Å). These small lattice mismatches enable the epitaxial formation of cubic Ni seed crystals on the substrate, leading the vertical growth of Ni NWs. Meanwhile, when the Ni (001) plane is rotated to an angle of 45°, domain-matched misfits of 0.32% and 4.03% appear along the Ni [110]//Al₂O₃ <1 $\bar{1}$ 00> and Ni [$\bar{1}$ 10]//Al₂O₃ <11 $\bar{2}$ 0> directions, respectively (Fig. S3†). This fair domain matching epitaxy can cause the formation of 45°-rotated Ni seed crystals, as shown in the cyan circles of Fig. 2a. The result of domain matching epitaxy explains well the two orientations of the cubic Ni seed crystals and further confirms that the vertical Ni NWs grow from cubic Ni seeds.

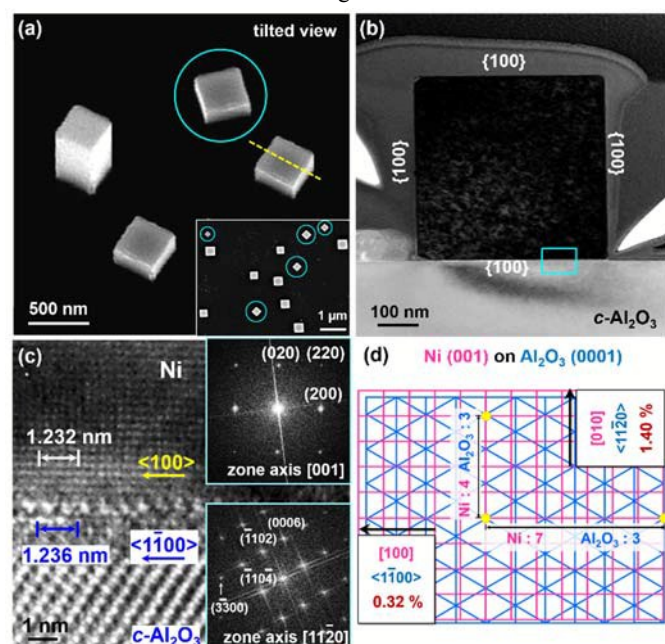


Fig. 2 (a) 35°-tilted SEM image of cubic Ni seed crystals on a *c*-Al₂O₃ substrate. The cubic Ni seed crystals have two types of orientations with an angle of 45°. The inset is a top-view SEM image of cubic Ni seed crystals. (b) Cross-sectional TEM image of a cubic Ni seed crystal after it was cut along the yellow dashed line in (a). (c) HRTEM image and FFT patterns of the cyan square region in (b). The lattice spacing of the Ni (100) planes is 1.76 Å and that of the Al₂O₃ (1 $\bar{1}$ 00) planes is 4.12 Å. (d) Schematic of the atomic planes at the epitaxial interface between the Ni (001) and Al₂O₃ (0001) planes.

Around the inclined Ni NWs, tetrahedral Ni seed crystals are observed. Fig. 3a and 3b show top view and 35°-tilted SEM images of tetrahedral Ni seeds. As shown in the red and yellow circles of Fig. 3a, the tetrahedral Ni seed crystals have two types of orientations and both Ni seeds are mirror images each other. Fig. 3c is a 35°-tilted SEM image of short inclined Ni NWs. The same alignments and tip structures of the inclined Ni NWs and tetrahedral Ni seed crystals suggest that the inclined Ni NWs grow from tetrahedral Ni seeds. Fig. 3d is a cross-sectional TEM image of a single tetrahedral Ni seed crystal cut along the yellow dashed line in Fig. 3a. This result shows that the tetrahedral Ni seed crystal is enclosed by {100} side facets and a (111) bottom plane. Fig. 3e shows an HRTEM image and the FFT pattern of the cyan square region in Fig. 3d, which suggests that the Ni (111) plane is formed epitaxially on the Al₂O₃ (0001) plane. The schematic of the atomic planes at the

epitaxial interface between the Ni (111) and Al₂O₃ (0001) planes shows that the misfits of 4.42% and 4.41% appear along the Ni <1 $\bar{1}$ 0>//Al₂O₃ <11 $\bar{2}$ 0> and Ni <11 $\bar{2}$ >//Al₂O₃ <1 $\bar{1}$ 00> directions, respectively (Fig. 3f, the lattice spacing of the Ni (1 $\bar{1}$ 0), Al₂O₃ (11 $\bar{2}$ 0), Ni (11 $\bar{2}$), and Al₂O₃ (1 $\bar{1}$ 00) planes are 2.49 Å, 2.38 Å, 4.31 Å, and 4.12 Å, respectively). The lattice mismatches of 4.42% and 4.41% are substantial. Nevertheless, tetrahedral Ni seed crystals are formed on the *c*-Al₂O₃ substrates because the same 3-fold symmetry of the Ni (111) and Al₂O₃ (0001) planes significantly reduce the interfacial energy between them.^{26,27}

We tried to find intermediate steps between tetrahedral Ni seeds and inclined Ni NWs. Ni nanocrystals in Fig. S4 (b, d, f) and (a, d, e) have very similar geometries and alignments as well as the same crystallographic structures, suggesting that the inclined Ni NWs grow from these Ni nanocrystals. The tilt angle of inclined Ni nanorods to the substrate is measured as 55°, which is the supposed tilt angle of the NWs.

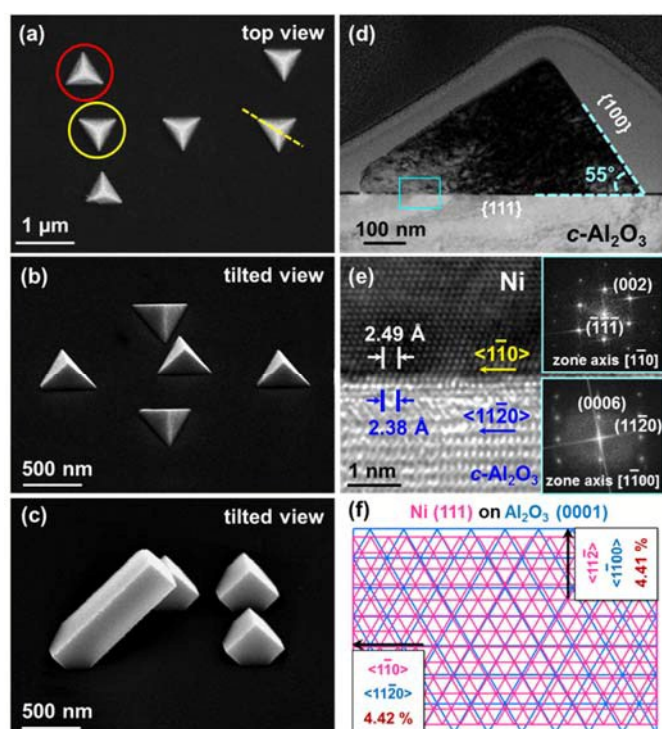


Fig. 3 (a) Top-view and (b) 35°-tilted SEM images of tetrahedral Ni seed crystals on a *c*-Al₂O₃ substrate. Tetrahedral Ni seed crystals have two types of orientations as marked by the red and yellow circles in (a). (c) 35°-tilted SEM image of the short inclined Ni NWs. (d) Cross-sectional TEM image of a tetrahedral Ni seed crystal after it was cut along the yellow dashed line in (a). (e) HRTEM image and FFT patterns of the cyan square region in (b). The lattice spacing of the Ni (1 $\bar{1}$ 0) planes is 2.49 Å and that of the Al₂O₃ (11 $\bar{2}$ 0) planes is 2.38 Å. (f) Schematic of atomic planes at the epitaxial interface between the Ni (111) and Al₂O₃ (0001) planes.

The deposition flux, substrate temperature, and local flow conditions are the key experimental conditions, strongly depending on the location at the substrate. Ni vapor flux is nearly perpendicular to the substrate at the center of the substrate, whereas turbulent vapor flow might occur at the edge of the substrate.²² When the Ni vapor flux direction is perpendicular to the substrate, vertical growth from the cubic seed could be more favored than inclined growth from the tetrahedral seed because of more favorable solid angle of collision

for the NW growth. Inclined NW growth could be more favored near the edge because of the turbulent flow.

3.3 Vertical Ni nanoplates on *r*-Al₂O₃ substrates

Ni nanoplates were vertically synthesized on *r*-Al₂O₃ substrates (Fig. 4a). The well-faceted Ni nanoplates are isosceles triangle shaped with 5–8 μm of bottom lengths and 2–4 μm of heights. Some of the Ni nanoplates are rotated by 86°, as shown in Fig. 4b. Fig. 4c–e show TEM and HRTEM images and the FFT pattern of a single Ni nanoplate. Distinct lattice fringes and a single set of face-centered cubic (fcc) Ni structures clearly confirm the single-crystallinity of the Ni nanoplates. The growth direction of vertical Ni nanoplates is [110]. The X-ray diffraction (XRD) patterns of both the Ni NWs and Ni nanoplates exhibit the same peaks, corresponding well with fcc Ni structure (JCPDS 7440-02-0, Fig. S5†).

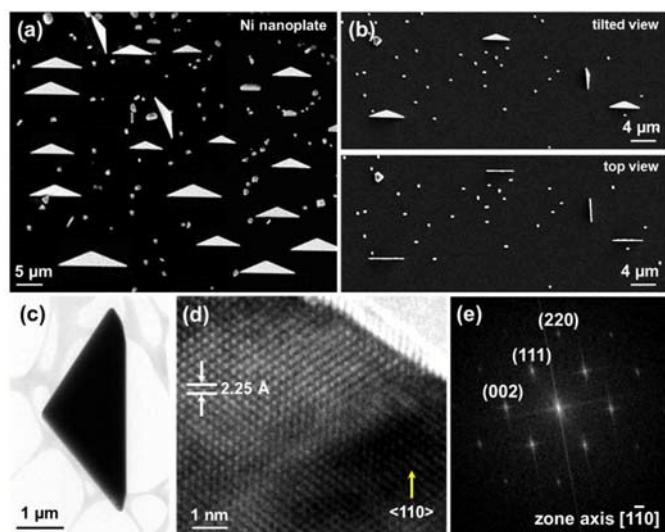


Fig. 4 (a) 35°-tilted SEM images of vertical Ni nanoplates on an *r*-Al₂O₃ substrate. Well-faceted Ni nanoplates have 5–8 μm bottom lengths, 2–4 μm heights, and isosceles triangle shapes. (b) 35°-tilted (upper) and top-view (lower) SEM images of vertical Ni nanoplates show that they have two types of orientations with an angle of 86°. (c) TEM and (d) HRTEM images and (e) FFT patterns of a Ni nanoplate show distinct lattice fringes and a single set of fcc Ni structure, verifying the single-crystallinity of the Ni nanoplates.

On the Ni nanoplate grown *r*-Al₂O₃ substrates, triangular Ni seed crystals are observed. Fig. 5a and its inset are 35°-tilted and top view SEM images of the triangular Ni seed crystals. The cyan dashed lines in Fig. 5a show that the triangular Ni seeds have two orientations with an angle of 86°. These orientations correspond to the vertical Ni nanoplates in Fig. 4b. The same alignments of vertical Ni nanoplates and triangular Ni seed crystals suggest that the vertical Ni nanoplates grow from the triangular Ni seeds. Fig. 5b is a cross-sectional TEM image of a single triangular Ni seed crystal cut along the yellow dashed line in Fig. 5a. The triangular Ni seed crystal is single-crystalline and enclosed by {100} side facets and a (110) bottom plane. The HRTEM image and FFT patterns of the cyan square region in Fig. 5b show that the Ni (110) plane is formed epitaxially on the Al₂O₃ ($\bar{1}012$) plane. Two layers of Ni and 1 layer of Al₂O₃ have 0.57% domain-matched misfit along the Ni <001>//Al₂O₃ <02 $\bar{2}$ 1> direction (Fig. 5d, the lattice spacing of the Ni (001) plane is 1.76 Å and that of the Al₂O₃ (02 $\bar{2}$ 1) plane is 3.50

Å). Additionally, 7 layers of Ni and 5 layers of Al₂O₃ have 0.40% domain-matched misfit along the Ni <110>//Al₂O₃ <2 $\bar{2}$ 01> direction (Fig. 5d, the lattice spacing of the Ni (110) planes is 2.49 Å and that of the Al₂O₃ (2 $\bar{2}$ 01) planes is 3.50 Å). These domain-matched misfits are small enough to form the triangular Ni seed crystals on *r*-Al₂O₃ substrates. Furthermore, the Al₂O₃ (02 $\bar{2}$ 1) and Al₂O₃ (2 $\bar{2}$ 01) planes have the same lattice spacing and they are angled 86° to each other. Therefore, Ni atoms can settle equally along the Ni <001>//Al₂O₃ <02 $\bar{2}$ 1> and Ni <001>//Al₂O₃ <2 $\bar{2}$ 01> directions, which is why the vertical Ni nanoplates have two orientations with an angle of 86° on *r*-Al₂O₃ substrates (Fig. S7†).

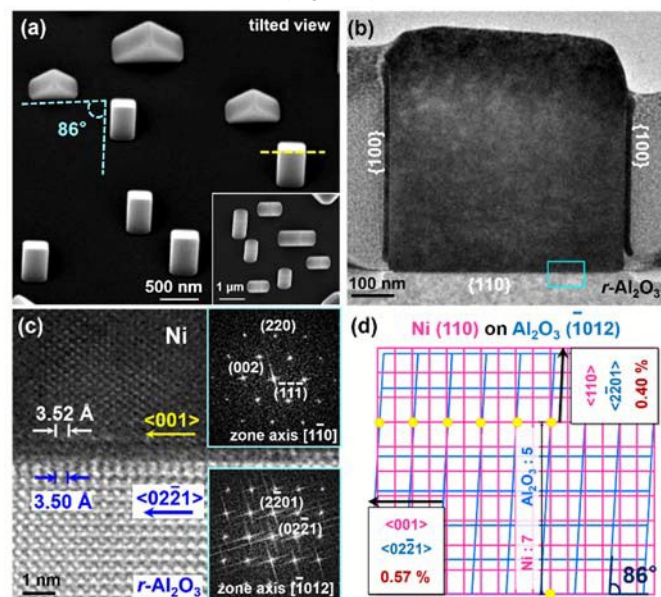
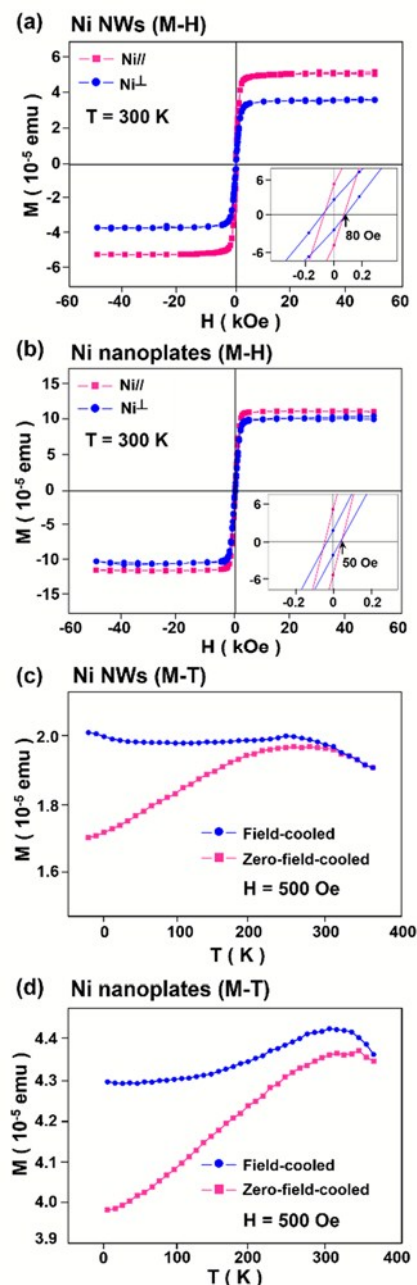


Fig. 5 (a) 35°-tilted SEM image of triangular Ni seed crystals on an *r*-Al₂O₃ substrate. Triangular Ni seed crystals have two types of orientations with an angle of 86°. The inset is a top-view SEM image of the triangular Ni seed crystals. (b) Cross-sectional TEM image of a triangular Ni seed crystal after it was cut along the yellow dashed line in (a). (c) HRTEM image and FFT patterns of the cyan square region in (b). The lattice spacing of the Ni (001) planes is 1.76 Å and that of the Al₂O₃ (02 $\bar{2}$ 1) planes is 3.50 Å. (d) Schematic of the atomic planes at the epitaxial interface between the Ni (110) and Al₂O₃ ($\bar{1}012$) planes.

We propose the following explanation for the growth mechanism of vertical Ni NWs, inclined Ni NWs, and vertical Ni nanoplates. The anisotropic growth of Ni nanostructures could be induced by the anisotropic environment that provides anisotropic flows of Ni vapor to the seed crystals, as we reported previously on noble metal NWs.²⁴ In the current experiment, NiCl₂ precursor can decompose to Ni vapor and chloride gas at 700 °C and 1 atm. Ni atoms colliding with the substrate nucleate to form small seed crystals, of which bottom planes are well matched with the lattice plane of the substrates. Ni atoms then directly deposit onto the pre-formed seed crystals or indirectly approach the seed crystals through surface diffusion after they first collide on the sapphire substrates. Since most of Ni NWs and Ni nanoplates are formed in vertical or inclined orientations on Al₂O₃ substrates, we suggest that direct impingement from the vapor is dominant when the substrate temperature is 850 ~ 900 °C. As we increased the substrate temperature higher than 1,000 °C, vertically grown Ni nanobelts were formed on *c*-Al₂O₃ substrates (Fig. S8†), these nanobelts are thought to be formed by

the lateral growth of Ni NWs due to increased surface diffusion of Ni atoms. When we increased initial amount of NiCl₂ precursor by three times (other experimental conditions were unchanged), Ni NWs were grown horizontally on *c*-Al₂O₃ substrates while short Ni nanorods were grown on *r*-Al₂O₃ substrates (Fig. S9†). These observations suggest that we can adjust the orientation of Ni nanostructures by controlling the magnitude of the deposition flux, which determines the dominant material flux direction toward the seed and thus the growth direction.



3.4 Magnetic property of vertical Ni nanowires and nanoplates

Fig. 6 M-H curves of vertical (a) Ni NWs and (b) nanoplates collected at 300 K. Distinct magnetic hysteresis loops are clearly shown. Ni// and Ni[⊥] imply that the external magnetic field is oriented in the parallel or perpendicular direction relative to the vertical Ni nanostructures. The insets of (a, b) are magnified hysteresis loops. The coercivity values of the Ni NWs and the nanoplates are 80 and 50 Oe. The M-T curves of the vertical (c) Ni NWs and (d) nanoplates show that they have T_B values greater than 300 K at 500 Oe.

The magnetic properties of the vertical Ni NWs and the Ni nanoplates were investigated using superconducting quantum interference device (SQUID) measurements. Fig. 6a and 6b are the M-H curves of vertical Ni NWs and nanoplates at 300 K. The curves show distinct magnetic hysteresis due to the structural anisotropy of the vertical Ni NWs and nanoplates. Ni// means that the external magnetic field is oriented in the parallel direction to the vertical Ni nanostructures, and Ni[⊥] means that the external magnetic field is oriented in the perpendicular direction to the vertical Ni nanostructures. In both applied field directions, the vertical Ni NWs and nanoplate exhibit typical ferromagnetic behavior. According to previous literatures, natural thin nickel-oxide layers may induce additional magnetic anisotropy via the exchange-bias effect at the ferromagnetic/antiferromagnetic interface (Fig. S10†).^{28,29} The insets of Fig. 6a and 6b are magnified hysteresis loops of the vertical Ni NWs and the nanoplates, showing that the coercivity values of the NWs and nanoplates are 80 and 50 Oe, respectively. Importantly, the M-T curves of vertical Ni NWs and nanoplates show that as-synthesized Ni nanostructures have blocking temperatures (T_B) greater than 300 K under an external magnetic field of 500 Oe (Fig. 6c and 6d). In previous reports, Ni nanoparticles with diameters of a few nanometers and triangular Ni nanoplates with edge lengths of ~15 nm exhibited T_B values of ~31 K and ~226 K at 500 Oe, respectively.³⁰⁻³² Our single-crystalline Ni NWs and nanoplates are much larger than these nanostructures and have a very clean surface without surfactants, thus they can form relatively large magnetic DWs and have strong magnetic anisotropy properties. Xu *et al.* reported that Ni nanoplatelets show T_B values higher than nanoparticles, which may be ascribed to the large size as well as good crystallinity.³³

Our vertical Ni NWs and nanoplates exhibit enhanced coercive force as a reflection of the magnetic shape anisotropy at room temperature compared with that of the bulk one (ca. 0.7 Oe). Single crystalline Ni NWs synthesized here also show higher magnetic properties than polycrystalline Ni NWs that can be considered as random-anisotropy ferromagnets, of which local uniaxial anisotropy competes with the interatomic exchange and external fields.³⁴

4. Conclusions

We developed the morphology and growth direction controllable synthetic method of Ni nanostructures in vapor phase. By using this method, vertical Ni NWs, inclined Ni NWs, and vertical Ni nanoplates were successfully synthesized on sapphire substrates. The morphology and growth direction of Ni nanostructures are determined by Ni seed crystals. Cubic Ni seeds grew into vertical Ni NWs, tetrahedral Ni seeds grew into inclined Ni NWs, and triangular Ni seed grew into vertical Ni nanoplates. Furthermore, vertical Ni NWs and nanoplates have blocking temperature values greater than 300 K at 500 Oe, verifying that these Ni nanostructures can form large magnetic DWs with high magnetic anisotropy properties. We expect that stereo-aligned Ni NWs and nanoplates will contribute to the development of 3-dimensional magnetic devices.

Acknowledgements

B.K. acknowledges support of this work from NRF grant (NRF-2013R1A2A2A01069073) and the Public welfare & Safety research program (NRF-2012M3A2A1051686) funded by the Ministry of Science, ICT and Future Planning, Korea. TEM analysis was performed at KBSI in Daejeon.

References

- G. A. Prinz, *Science* 1998, **282**, 1660–1663.
- A. Brataas, A. D. Kent, H. Ohno, *Nat. Mater.* 2012, **11**, 372–381.
- S. S. P. Parkin, M. Hayashi, L. Thomas, *Science* 2008, **320**, 190–194.
- I. Takeuchi, O. O. Famodu, J. C. Read, M. A. Aronova, K. -S. Chang, C. Craciunescu, S. E. Lofland, M. Wuttig, F. C. Wellstood, L. Knauss, A. Orozco, *Nat. Mater.* 2003, **2**, 180–184.
- J. Cui, Y. S. Chu, O. O. Famodu, Y. Furuya, J. Hattrick-Simpers, R. D. James, A. Ludwig, S. Thienhaus, M. Wuttig, Z. Zhang, I. Takeuchi, *Nat. Mater.* 2006, **5**, 286–290.
- Y. Tanaka, Y. Himuro, R. Kainuma, Y. Sutou, T. Omori, K. Ishida, *Science* 2010, **327**, 1488–1490.
- I. S. Lee, N. Lee, J. Park, B. H. Kim, Y. W. Yi, T. Kim, T. K. Kim, I. H. Lee, S. R. Paik, T. Hyeon, *J. Am. Chem. Soc.* 2006, **128**, 10658–10659.
- V. Bonanni, S. Bonetti, T. Pakizeh, Z. Pirzadeh, J. Chen, J. Nogués, P. Vavassori, R. Hillenbrand, J. Åkerman, A. Dmitriev, *Nano Lett.* 2011, **11**, 5333–5338.
- A. Atkinson, S. Barnett, R. J. Gorte, J. T. S. Irvine, A. J. McEvoy, M. Mogensen, S. C. Singhal, J. Vohs, *Nat. Mater.* 2004, **3**, 17–27.
- J. R. Wilson, W. Kobsiriphat, R. Mendoza, H. -Y. Chen, J. M. Hiller, D. J. Miller, K. Thornton, P. W. Voorhees, S. B. Adler, S. A. Barnett, *Nat. Mater.* 2006, **5**, 541–544.
- G. W. Huber, J. W. Shabaker, J. A. Dumesic, *Science* 2003, **300**, 2075–2077.
- A. L. Goff, V. Artero, B. Jusselme, P. D. Tran, N. Guillet, R. Métayé, A. Fihri, S. Palacin, M. Fontecave, *Science* 2009, **326**, 1384–1387.
- S. Scheller, M. Goenrich, R. Boecher, R. K. Thauer, B. Jaun, *Nature* 2010, **465**, 606–608.
- C. D. Wessells, S. V. Peddada, R. A. Huggins, Y. Cui, *Nano Lett.* 2011, **11**, 5421–5425.
- X. W. Wang, G. T. Fei, X. J. Xu, Z. Jin, L. D. Zhang, *J. Phys. Chem. B* 2005, **109**, 24326–24330.
- H. Pan, B. Liu, J. Yi, C. Poh, S. Lim, J. Ding, Y. Feng, C. H. A. Huan, J. Lin, *J. Phys. Chem. B* 2005, **109**, 3094–3098.
- C. M. Hangarter, N. V. Myung, *Chem. Mater.* 2005, **17**, 1320–1324.
- F. Li, M. Zhu, C. Liu, W. L. Zhou, J. B. Wiley, *J. Am. Chem. Soc.* 2006, **128**, 13342–13343.
- K. T. Chan, J. J. Kan, C. Doran, L. Ouyang, D. J. Smith, E. E. Fullerton, *Nano Lett.* 2010, **10**, 5070–5075.
- K. T. Chan, J. J. Kan, C. Doran, L. Ouyang, *Philosophical Magazine* 2012, **92**, 2173–2186.
- N. Liakakos, C. Achkar, B. Cormary, J. Harmel, B. Warot-Fonrose, E. Snoeck, B. Chaudret, M. Respaud, K. Soulantica, T. Blon, *ACS Nano* 2015, ASAP (DOI: 10.1021/acsnano.5b04524).
- Y. Yoo, S. Han, M. Kim, T. Kang, J. In, B. Kim, *Chem. Asian J.* 2011, **6**, 2500–2505.
- A. E. van Arkel, J. H. Boer, *Z. Anorg. Allg. Chem.* 1925, **148**, 345–350.
- Y. Yoo, K. Seo, S. Han, K. S. K. Varadwaj, H. Kim, J. Ryu, H. Lee, J. Ahn, H. Ihee, B. Kim, *Nano Lett.* 2010, **10**, 432–438.
- J. Narayan, B. C. Larson, *J. Appl. Phys.* 2003, **93**, 278–285.
- T. Nakamura, H. Minoura, H. Muto, *Thin Solid Films* 2002, **405**, 109–116.
- G. Dehm, M. Rühle, G. Ding, R. Raj, *Philosophical magazine B* 1995, **71**, 1111–1124.
- N. Bagkar, K. Seo, H. Yoon, J. In, Y. Jo, B. Kim, *Chem. Mater.* 2010, **22**, 1831–1835.
- V. Salgueiriño-Maceira, M. A. Correa-Duarte, M. Bañobre-López, M. Grzelczak, M. Farle, L. M. Liz-Marzán, J. Rivas, *Adv. Funct. Mater.* 2008, **18**, 616–621.
- M. J. Bonder, E. M. Kirkpatrick, T. Martin, S. -J. Kim, R. D. Rieke, D. L. Leslie-Pelecky, *J. Magn. Magn. Mater.* 2000, **222**, 70–78.
- Y. Leng, Y. Li, X. Li, S. Takahashi, *J. Phys. Chem. C* 2007, **111**, 6630–6633.
- C. L. Yuan, *J. Phys. Chem. C* 2010, **114**, 2124–2126.
- R. Xu, T. Xie, Y. Zhao, Y. Li, *Crystal Growth & Design* 2007, **7**, 1904–1911.
- M. Zheng, L. Menon, H. Zeng, Y. Liu, S. Bandyopadhyay, R. D. Kirby, D. J. Sellmyer, *Phys. Rev. B* 2000, **62**, 12282–12286.

TOC

Vertical Ni NWs, inclined Ni NWs, and vertical Ni nanoplates were epitaxially grown on sapphire substrates with single-crystalline structure in vapor phase. The morphology and growth direction of Ni nanostructures are determined by Ni seed crystals.

